applied sciences

MDPI

Article

Intelligent Fault Diagnosis of Rotating Machinery Using Hierarchical Lempel-Ziv Complexity

Bing Han [1], Shun Wang [2], Qingqi Zhu [1], Xiaohui Yang [1] and Yongbo Li [2,*]

[1] Shaanxi Engineering Laboratory for Transmissions and Controls, Northwestern Polytechnical University, Xi'an 710072, China; npuhanbing@nwpu.edu.cn (B.H.); 1115012259@mail.nwpu.edu.cn (Q.Z.); yangxh@nwpu.edu.cn (X.Y.)

[2] MIIT Key Laboratory of Dynamics and Control of Complex System, School of Aeronautics, Northwestern Polytechnical University, Xi'an 710072, China; wangshun@mail.nwpu.edu.cn

* Correspondence: yongbo@nwpu.edu.cn; Tel.: +86-1880-918-3733

Received: 11 May 2020; Accepted: 17 June 2020; Published: 19 June 2020

check for updates

Abstract: The health condition monitoring of rotating machinery can avoid the disastrous failure and guarantee the safe operation. The vibration-based fault diagnosis shows the most attractive character for fault diagnosis of rotating machinery (FDRM). Recently, Lempel-Ziv complexity (LZC) has been investigated as an effective tool for FDRM. However, the LZC only performs single-scale analysis, which is not suitable to extract the fault features embedded in vibrational signal over multiple scales. In this paper, a novel complexity analysis algorithm, called hierarchical Lempel-Ziv complexity (HLZC), was developed to extract the fault characteristics of rotating machinery. The proposed HLZC method considers the fault information hidden in both low-frequency and high-frequency components, resulting in a more accurate fault feature extraction. The superiority of the proposed HLZC method in detecting the periodical impulses was validated by using simulated signals. Meanwhile, two experimental signals were utilized to prove the effectiveness of the proposed HLZC method in extracting fault information. Results show that the proposed HLZC method had the best diagnosing performance compared with LZC and multi-scale Lempel-Ziv complexity methods.

Keywords: feature extraction; fault diagnosis; Lempel-Ziv complexity; rotating machinery

1. Introduction

Rotating machinery is commonly used in modern industries, such as the aero-engine, vehicle, ship, and railway industries [1]. In industrial applications, the strict working environment may result in localized damage on rotating machinery. If the damage cannot be timely diagnosed, it may cause disastrous failure and serious economic loss. Therefore, it is crucial to conduct the fault diagnosis of rotating machinery (FDRM) so as to ensure its safety operation [2].

Until now, many advanced techniques have been developed to accomplish the FDRM, such as the vibration-based fault diagnosis method [3,4], acoustic emission-based fault diagnosis method [5,6], and rotary encoder-based fault diagnosis method [7]. Among these techniques, the vibration signal method is most widely applied in industrial applications due to the its advantage of easy measurement and high scalability [8]. Generally, three main stages are included in the vibration-based method: data collection, fault feature extraction, and pattern identification. During the three stages, the fault feature extraction lays a good foundation for FDRM. Some advanced fault feature approaches have been proposed for the FDRM, such as blind source separation [9], wavelet-based method [10], and adaptive decomposition methods [11].

Unfortunately, the complex dynamical structure and complex operating conditions of rotating machinery often generate nonlinear and non-stationary characteristics in the measured vibration signals, resulting in the difficulty in extracting the weak fault characteristics from the vibration signals [12]. Thanks to the rapid development of complexity theory, some complexity indexes are used to extract fault features of rotating machinery, such as Lempel-Ziv complexity (LZC) [13], approximate entropy [14], fuzzy entropy [12,15], permutation entropy [16,17], symbolic dynamic entropy [18], and multi-scale entropy [19]. Related research have indicated that LZC is powerful in analyzing vibration signals of mechanical systems. Yan et al. [13] used LZC to distinguish different bearing failure severity. Hong et al. [20] calculated LZC after wavelet transformation to recognize the fault severity of bearing. Cui et al. [21] proposed a signal decomposition and reconstruction method based on LZC and the double-dictionary matching pursuit. Meanwhile, Cui et al. [22] proposed a fault diagnosis method that was based on Sparsogram and LZC. Moreover, Bai et al. [23] utilized the permutation of the LZC to quantify the complexity of the signal, whereas Yin et al. [24] proposed a novel symbolic aggregate approximation and LZC method for fault diagnosis of rolling bearings.

However, the existing LZC methods have one common problem when analyzing the vibration signals. Since the fault information is usually embedded in vibration signals over different scale domains [25], the LZC-based methods only perform single-scale analysis, and thus the fault characteristics cannot be comprehensively described. In order to match the fault characteristics comprehensively, we proposed multi-scale Lempel-Ziv complexity (MLZC) to extract the fault features over multiple scales by multi-scale analysis [26]. However, the coarse-grained process is actually a linear smoothing process, which only considers the low-frequency components through the averaging process, and thus the fault information of the high-frequency component is discarded. In actual application, the fault information is embedded in both the low–high and high-frequency components of measured vibration signal. For example, a real vibration signal and its corresponding frequency spectrum are shown in Figure 1a,b, respectively. As can be seen, both the low-frequency (0–500 Hz) and high-frequency (2500–3500 Hz) components contain the main fault information of rotating machinery. Therefore, the fault extraction performance of MLZC still needs to be improved.

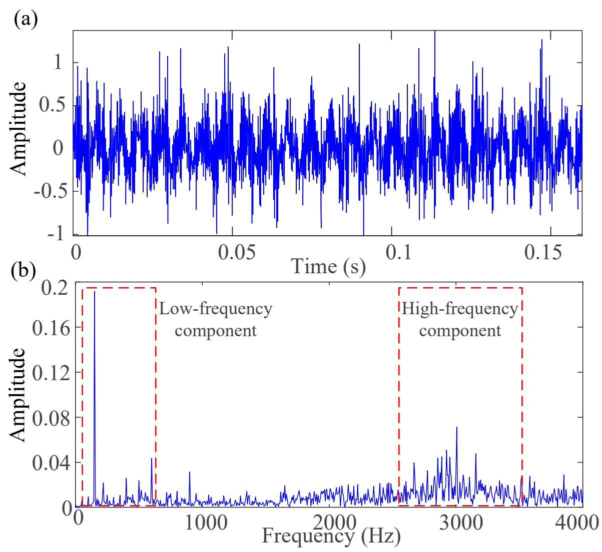

Figure 1. (**a**) The waveform of measured rating machinery vibration signals, and (**b**) its corresponding frequency spectrum.

To overcome such defects, this paper developed a novel approach called hierarchical Lempel-Ziv complexity (HLZC) to quantify the complexity from the measured time series. Compared with the MLZC method, HLZC utilizes both the low-frequency components generated by averaging the components and the high-frequency components generated by taking the difference of components to produce the sub time series in each layer. The merits of our proposed HLZC method in fault feature extraction are verified using both synthetic signals and experimental signals. Results demonstrated that our proposed HLZC method is superior to LZC and MLZC in extracting fault characteristics with high stability. After the HLZC-based feature extraction, we combined the HLZC with support vector machine (SVM) classifier [27] to accomplish the intelligent fault diagnosis of rotating machinery.

The remainder of this paper is organized as follows. Section 2 introduces the fundamentals of our proposed HLZC method. Moreover, the superiority of HLZC is validated using simulated impulsive signal through comparing with LZC and MLZC methods. Section 3 describes the framework of HLZC-based intelligent fault diagnosis method. Section 4 provides the experimental variation using two case studies. Finally, Section 5 draws the final conclusion of this paper.

2. Proposed Hierarchical Lempel-Ziv Complexity

2.1. Lempel-Ziv Complexity

LZC, as a nonlinear method, has been proven to be an efficient tool to measure the complexity for a given time series. LZC consists of two basic operations: copy and insert [20]. The LZC algorithm can be detailed as

(1) Cover the finite sequence $x(t)$ into 0–1 sequence by comparing with the median value T_d using Equation (1). Then, we can obtain the symbol series $S_N = \{s_1 s_2 \ldots s_N\}$.

$$s_i = \begin{cases} 0, \text{ if } x(i) < T_d \\ 1, \text{ otherwise} \end{cases} \tag{1}$$

(2) Set the initial value $S_{v,0} = \{\}$, $Q_0 = \{\}$, $C_N(0) = 0$, and $i = 1$. Note that S_v and Q represent the substrings of the symbol series S_N, and C_N represents complexity counter.

(3) Let $Q_i = \{Q_{i-1} s_i\}$ and judge whether Q_i belongs to $S_{v,i-1} = \left\{S_{v,i-2} s_{i-1}\right\}$. If so, set $C_N(i) = C_N(i-1)$ and $i = i+1$. Otherwise, set $Q_i = \{\}$, $C_N(i) = C_N(i-1) + 1$, and update $i = i+1$.

(4) Repeat Step (3) until the end of symbol series $S_N = \{s_1 s_2 \ldots s_N\}$, and then the $C_N(N)$ can be obtained. $C_N(N)$ is the last complexity counter, which reflects upon the number of all different subsequences contained in the original data sequence.

(5) Normalize the $C_N(N)$ to obtain relatively independent indicator $C_{n,N}$ using Equations (2) and (3).

$$C_{n,N} = \frac{C_N(N)}{C_{UL}} \tag{2}$$

$$C_{UL} = \lim_{N \to \infty} C_N(N) \approx \frac{N}{\log_2 N} \tag{3}$$

2.2. Multi-Scale Lempel-Ziv Complexity

On the basis of LZC and coarse-grained procedure [26], MLZC can be summarized into two steps. (1) Conduct the multiple series by the coarse-graining analysis; (2) calculate the LZC values of each coarse-grained time series.

(1) Given an arbitrary time series $X\{x(k), k = 1, 2, \cdots, N\}$, construct consecutive coarse-grained time series $\left\{y^{(\tau)}\right\}$ according to Equation (4).

$$y_j^\tau = \frac{1}{\tau} \sum_{i=(j-1)\tau+1}^{j\tau} x_i \quad 1 \le j \le \frac{N}{\tau} \tag{4}$$

where τ is a positive integer. The obtained coarse-grained time series $\left\{y^{(1)}\right\}$ is equal to the original time series when $\tau = 1$.

(2) Calculate the LZC for each coarse-grained time series according to the definition of LZC as written in Equation (5).

$$MLZC(x, \tau) = LZC(y^\tau) \tag{5}$$

The flowchart of MLZC is drawn in Figure 2. Additionally, we set the parameter scale τ = 20 in the paper. The parameter τ = 20 has been proven to be effective using experimental tests for multi-scale analysis in [12,15,18,28].

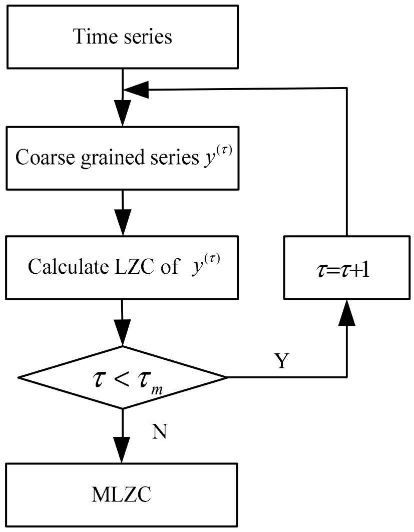

Figure 2. The flowchart of multi-scale Lempel-Ziv complexity (MLZC).

However, the MLZC algorithm only uses the low-frequency components generated by the multi-scale procedure for feature extraction, which unavoidably discards some useful fault information hidden in the high-frequency components. To address these shortcomings of MLZC, this paper developed a novel method called HLZC. First, the hierarchical decomposition is adopted to generate sub time series called hierarchical series. Second, the LZC values of all hierarchical nodes are all computed for comprehensive complexity estimation.

2.3. Hierarchical Lempel-Ziv Complexity

In this subsection, a novel method called HLZC is proposed by combining the hierarchical decomposition and Lempel-Ziv complexity. The hierarchical decomposition can decompose an arbitrary time series into high-frequency components and low-frequency components [29]. Figure 3 gives an example of the structure of hierarchical components decomposed by hierarchical decomposition. The detailed calculation procedures of our proposed HLZC method can be summarized into four steps as follows.

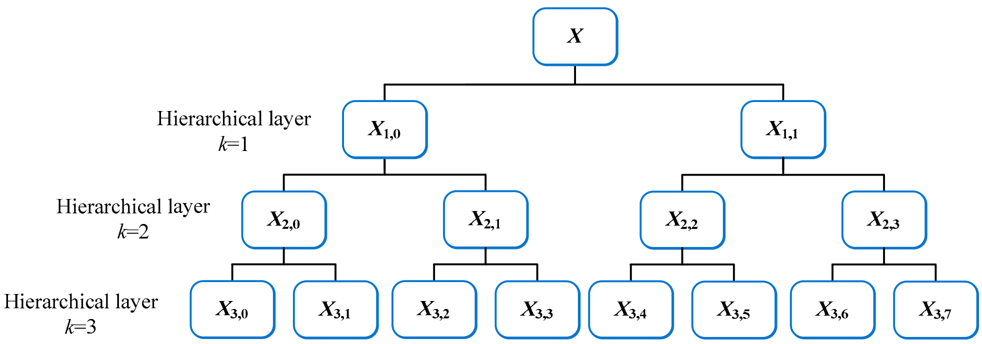

Figure 3. The structure of hierarchical components with three hierarchical layers.

(1) For an arbitrary time series $X\{x(i), i = 1, 2, \cdots, N\}$, the averaging operator Q_0 and differential operator Q_1 can be expressed as follows:

$$Q_0(x) = \frac{x(i) + x(i+1)}{2} \quad i = 1, 2, \cdots, N-1 \tag{6}$$

$$Q_1(x) = \frac{x(i) - x(i+1)}{2} \quad i = 1, 2, \cdots, N-1 \tag{7}$$

where $Q_0(x)$ and $Q_1(x)$ denote the low-frequency component and high-frequency component for a given time series, respectively.

(2) Conducting of the operators Q_j matrix (j = 0 or 1) can be adaptively generated according to the length of the time series N as follows:

$$Q_j = \begin{bmatrix} \frac{1}{2} & \frac{(-1)^j}{2} & 0 & 0 & \cdots & 0 & 0 \\ 0 & 0 & \frac{1}{2} & \frac{(-1)^j}{2} & \cdots & 0 & 0 \\ \vdots & \vdots & \vdots & \vdots & \vdots & \vdots & \vdots \\ 0 & 0 & 0 & 0 & \cdots & \frac{1}{2} & \frac{(-1)^j}{2} \end{bmatrix}_{N/2 \times N} \tag{8}$$

(3) Repeat step (2) to obtain the hierarchical components $X_{k,e}$ as Equation (9).

$$X_{k,e} = Q_{r_k}^{k} \cdot Q_{r_{k-1}}^{k-1} \cdot \cdots \cdot Q_{r_1}^{1} \cdot x \tag{9}$$

where e is the number of hierarchical nodes. For hierarchical layer k, e can be obtained as follows:

$$e = \sum_{m=1}^{k} 2^{k-m} r_m \tag{10}$$

where $[r_1, r_2 \cdots, r_k]$ represents the unique vector corresponding to the integer e, and $\{r_m, m = 1, \ldots, k\} \in \{0, 1\}$ indicates the averaging or differential operator at the kth layer.

(4) Compute all the hierarchical components by repeatedly using steps (1)–(3). Then, calculate LZC values of all the nodes. The HLZC is the set of all LZC values expressed as

$$HLZC(X, k) = LZC\left(X_{k,e}\right) \tag{11}$$

The calculation process of HLZC is shown in Figure 4.

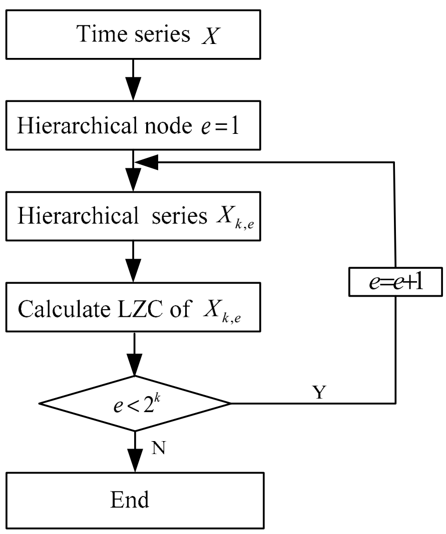

Figure 4. Flowchart of the hierarchical Lempel-Ziv complexity (HLZC) method.

2.4. Simulated Impulsive Signal

In this subsection, one impulsive signal was adopted to verify the advantage of proposed HLZC in detecting various fault types. Three different bearing fault types were utilized in the simulated signal: bearing with ball fault, bearing with inner race fault, and bearing with outer race fault. The number of sample points of the synthetic signal was 24,600, which was cut out by a sliding window of 2048 points with a step length of 256 points. Three simulated faulty bearing signals in time domains are shown in Figure 5a. For comparison purposes, LZC, MLZC, and HLZC were all utilized to process the impulsive signals. In this paper, three commonly used distance measures—Euclidean distance (ED), Chebychev distance (CD), and Minkowski distance (MD)—were all applied to verify the advantage of our proposed method in tracking the impulses. Note that we averaged the first 10 samples as normal samples. The distance value between each sample and normal samples was computed for comparisons. Here, we set the scale τ = 1:20 for MLZC and the number of hierarchical layers k = 4 for HLZC methods.

The obtained results are shown in Figures 5–7. Two conclusions can be drawn from Figures 5–7 as follows. First, it can be observed from (b) and (c) of three figures that the original LZC and MLZC could not detect the impulses derived from three different bearing fault types, resulting in failure of bearing feature extraction. In contrast, our proposed HLZC method not only identified three different bearing types by tracking the impulse, but also generated less fluctuation and high accuracy, as shown in (d) of the three figures. Second, the results using the three distance measures had a high consistency, and thus the fault detection ability of three methods can be listed as HLZC > MLZC > LZC. This further demonstrated that our proposed HLZC method has a significant advantage in fault feature extraction.

To explain the advantage of our proposed HLZC in detecting the impulses, we enlarged the bearing with outer race fault signal and conducted the fast Fourier transform (FFT) analysis. The time domain waveforms and its corresponding frequency spectra are shown in Figure 8a,b, respectively. As can be seen, the fault information was mainly located in the high-frequency component (1000–1500 Hz). The fault information embedded in the high-frequency component was ignored using the traditional MLZC method, resulting in worse impulsive detection performance. Compared with the MLZC method, HLZC utilized both averaging and differencing process to extract the fault information hidden in both low-frequency and the high-frequency components. Therefore, the proposed HLZC method generates the best performance in fault feature extraction.

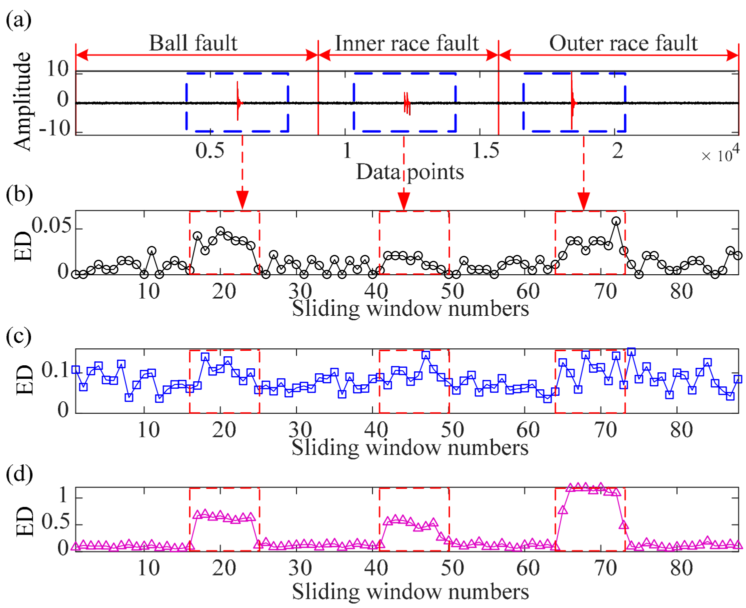

Figure 5. Results of sliding window analysis of Lempel-Ziv complexity (LZC), MLZC, and HLZC methods: (**a**) the simulated impulsive signal, (**b**) the Euclidean distance (ED) value of LZC, (**c**) the ED value of MLZC, and (**d**) the ED value of HLZC.

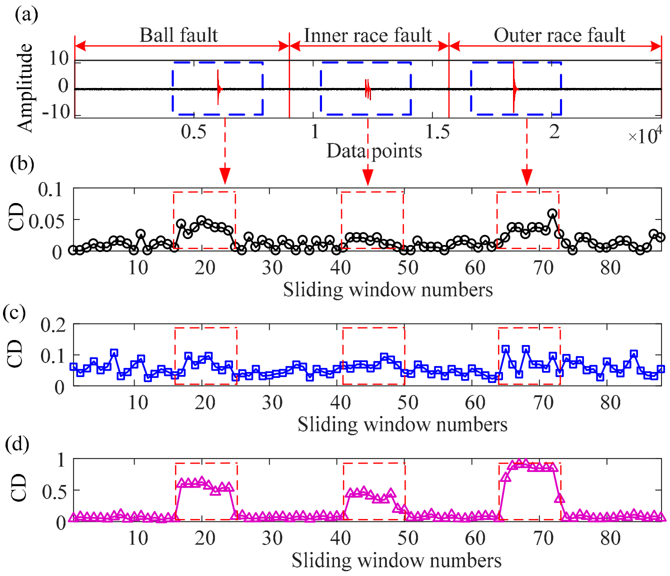

Figure 6. Results of sliding window analysis of LZC, MLZC, and HLZC methods with Chebychev distance (CD): (**a**) the simulated impulsive signal, (**b**) the CD value of LZC, (**c**) the CD value of MLZC, and (**d**) the CD value of HLZC.

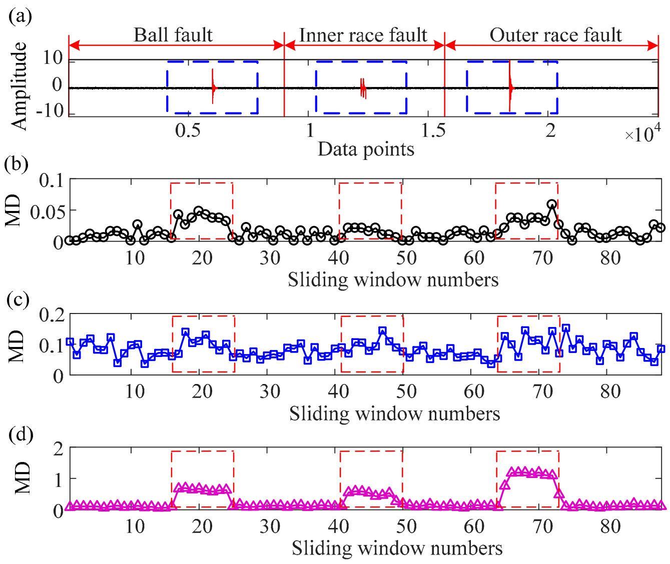

Figure 7. Results of sliding window analysis of LZC, MLZC, and HLZC methods with Minkowski distance (MD): (**a**) the simulated impulsive signal, (**b**) the MD value of MLZC, (**c**) the MD value of LZC, and (**d**) the MD value of HLZC.

Note that the fault frequency (BPFO) obtained using the envelope spectrum analysis was equal to the side band interval frequency of bearing intrinsic frequency in the conventional FFT method. First, the frequency spectrum using FFT could not detect the bearing fault frequency (BPFO) directly. It can be seen in Figure 8b that the bearing faults could be diagnosed by observing the intrinsic frequency and its harmonics. Second, we also conducted the envelope spectrum analysis. The fault frequency (BPFO) and its harmonics can be clearly observed in Figure 8c. Because the bearing fault can generate repetitive impulses, the measured vibration signal is thus a typical amplitude- and frequency-modulated (AM-FM) signal. The amplitude-modulated (AM) signal can be obtained by using envelope demodulated analysis, and then the fault frequency (BPFO) can be obtained by conducting the FFT on the AM signal.

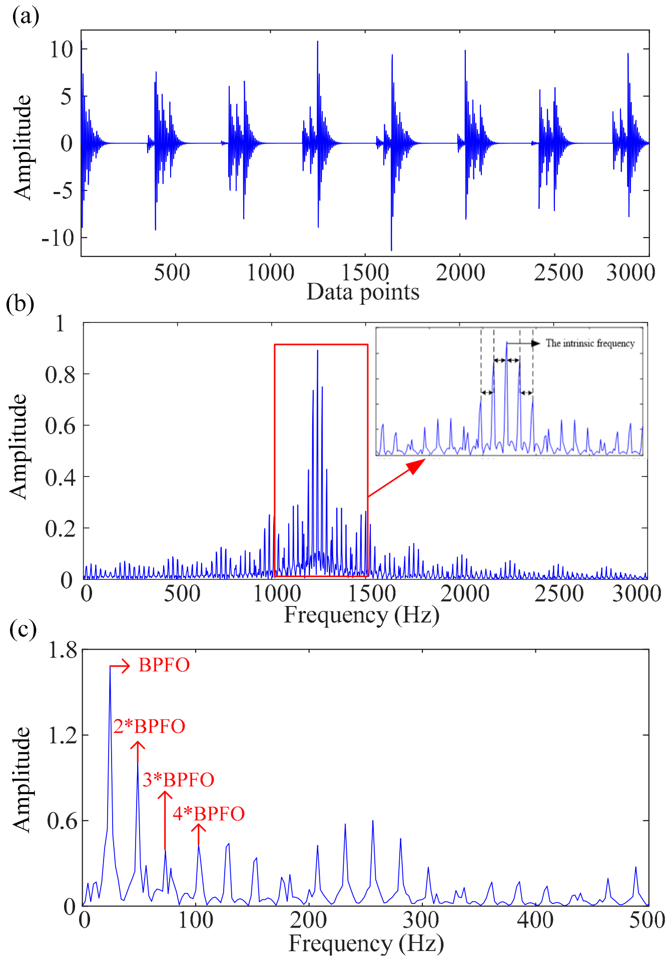

Figure 8. The simulated bearing signal with outer race fault: (**a**) the waveform, (**b**) its corresponding fast Fourier transform (FFT) spectrum, (**c**) the envelope spectrum.

3. Proposed Fault Diagnosis Framework

3.1. Support Vector Machine

In this paper, support vector machine (SVM) [30] was taken as the classifier to accomplish the pattern identification. SVM is a typical supervised learning method for recognition and regression analysis. The kernel function plays a significant role in the SVM classifier, which is not only important to reduce the computation cost but also useful in transforming the features into high dimension so as to construct the hyper-plane [28,31].

Three different used kernel functions of SVM consist of linear kennel function, polynomial kernel functions, and radial basis function (RBF) kernel function, which can be expressed as follows:

(1) Linear kernel

$$K(x, x_i) = < x{\cdot}x_i > \tag{12}$$

(2) Polynomial kernel

$$K(x, x_i) = (< x{\cdot}x_i > +c)^d \tag{13}$$

(3) Radial basis function (RBF) kernel

$$K(x, x_i) = \exp\left\{-\gamma\|x - x_i\|^2\right\} \tag{14}$$

where $\gamma > 0$, and γ is the kernel parameter.

Among these functions, the RBF function is most widely used due to its good performance, in which there are two parameters—penalty parameter C and kernel parameter γ—which require optimization. Here, the grid search method was utilized to optimize the two parameters [28]. It is worth mentioning that the dataset was randomly split into training and testing subsets through a k-fold cross-validation (CV). Every k subset takes turns to perform as an independent test set for the rest of the $(k-1)$ training subsets. The test sets being independent provides the necessary compensation for CV so as to enhance the consistency in the output. In this paper, the fivefold CV was adopted to adjust the model parameters. The coarse grid points were firstly selected through the exponential growing sequence 2^{-I} to 2^{+I}, where I is an integer. The optimal parameters for C and γ are assumed as (j, k), and the values are further optimized by using finer grid, in which the respective search area is $2^{j\pm f}$ and $2^{k\pm f}$. In this paper, we set the range of f as $-0.75 \leq f \leq 0.75$, with an interval of 0.25.

It is worth noticing that the one-against-one approach is applied to solve the multi-class classification problem in this paper [32]. To deal with the k number classes, the $k(k-1)/2$ SVM models are required for classification. For the present work, LIBSVM software package was used to deal with the multiple-fault diagnosis of rotating machinery.

3.2. Proposed Method

With the help of the advantages of HLZC and SVM, a novel intelligent fault diagnosis scheme called HLZC-SVM is proposed in this paper. There are two stages in the proposed intelligent fault diagnosis framework. In the first stage, HLZC is employed to extract the fault features from the vibration signals of rotating machinery. In the second stage, SVM is adopted to identify different fault types. Five steps are included in the FDRM method as follows:

(1) Measure the vibration data for various conditions of rotating machinery;
(2) Partition the measured vibration data into training datasets and testing datasets;
(3) Utilize HLZC to extract fault features from the vibration signals. Note that the hierarchical decomposition layers of HLZC is set as $k = 4$, and thus 31 features will be obtained;
(4) Train SVM classifier using the training features;
(5) Test the trained SVM classifier, wherein the output of SVM can be used to recognize the different fault types of rotating machinery.

The flowchart of the proposed fault diagnosis method is shown in Figure 9.

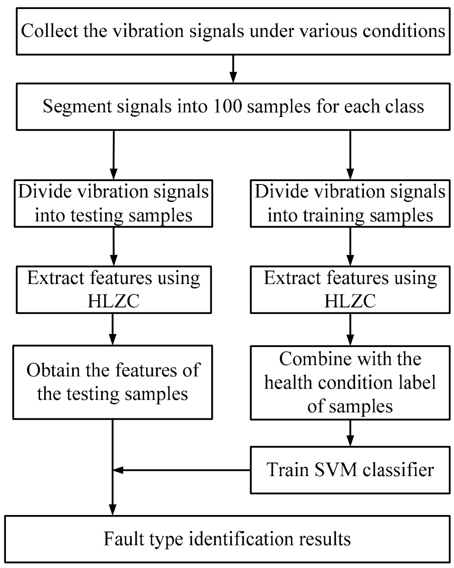

Figure 9. Flowchart of the proposed fault diagnosis method.

4. Experimental Validations

In order to validate the effectiveness of the proposed HLZC method in extracting the fault features, we designed two experiments in this paper. The two experiments were conducted on a fault simulator made by SpectraQuest called machinery fault simulator (MFS), which is drawn in Figure 10. The MFS consists of rolling bearings, a driven motor, and a three-way gearbox. At the rear of the gearbox, a magnetic clutch was used to generate the radial load. To collect the vibration data, we installed an acceleration transducer on the top of the gearbox. The rotating speed of the motor was kept at constant vale of 3000 rpm. Note that a 5 in-lbs of torque was added to simulate the machine load environment. The sampling frequency was 12,800 Hz. To simulate different faults, we replaced the test bearing and test gear by artificial damaged gear and artificial local damaged bearing, as shown in Figure 11.

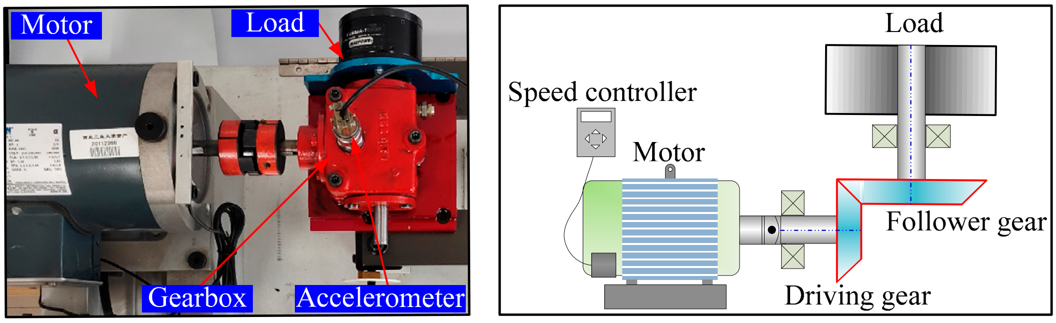

Figure 10. The experimental platform and its schematic diagram.

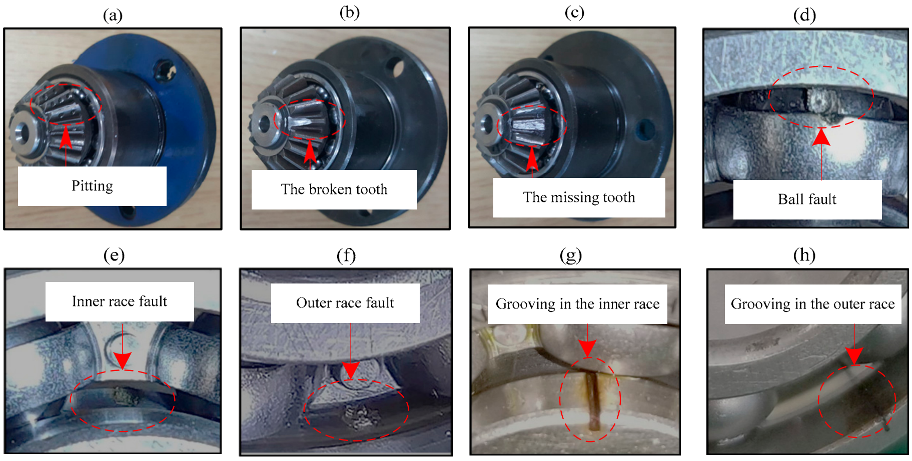

Figure 11. Faulty gears and bearings: (**a**) pitting in the driving tooth, (**b**) broken tooth in the driving tooth, (**c**) missing tooth in the driving tooth, (**d**) ball fault, (**e**) inner race fault, (**f**) outer race fault, (**g**) grooving in the inner race, (**h**) grooving in the outer race.

Experiment 1 aimed to show the superiority of the proposed HLZC method for single FDRM, which only covers single fault types of rotating machinery. Experiment 2 aimed to simulate the compound fault of rotating machinery including the bearing and gear fault, which was used to validate the superiority of the proposed HLZC method for compound FDRM. In this experiment, 50% of samples were randomly chosen as training samples, and the remainder of samples were used as testing samples. For comparison purposes, LZC and MLZC were all applied to process the data collected from the two experiments.

4.1. Experiment 1

Experiment 1 consisted of one healthy condition and five single fault conditions, including inner race fault (IRF), ball fault (BF), grooving in the inner race (GIR), grooving in the outer race (GOR), and outer race fault (ORF). There were 100 samples in each class and 600 samples in total. Meanwhile, the data length was 2048 points. The waveforms under six healthy conditions are shown in Figure 12. Table 1 gives the detailed information of six healthy conditions, including class label, damage diameter, and the numbers of training and testing data.

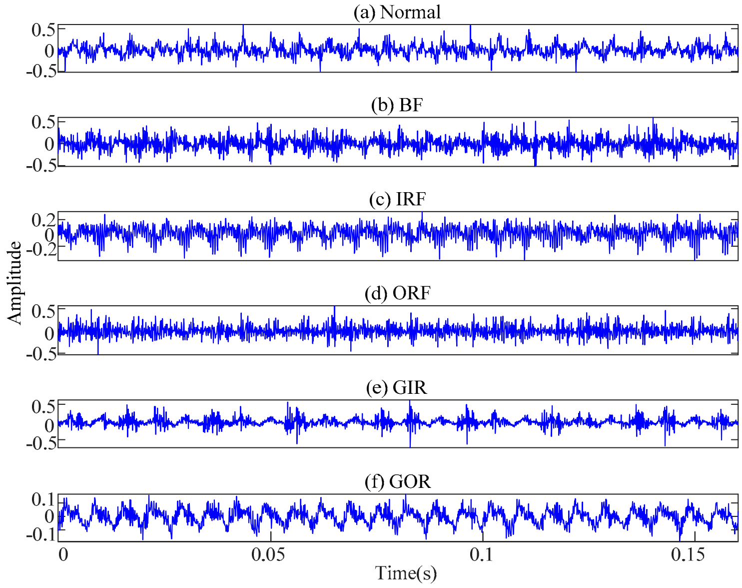

Figure 12. The time domain waveforms of rotating machinery under six healthy conditions in Experiment 1: (**a**) health condition (Normal), (**b**) ball fault (BF), (**c**) inner race fault (IRF), (**d**) outer race fault (ORF), (**e**) grooving in the inner race (GIR), (**f**) grooving in the outer race (GOR).

Table 1. Detailed information of six conditions in Experiment 1.

Fault Class	Class Label	Damage Diameter (mm)	Number of Training Samples	Number of Testing Samples
Normal	1	0	50	50
Ball fault	2	0.01	50	50
Inner race fault	3	0.01	50	50
Outer race fault	4	0.01	50	50
Grooving in the inner race	5	0.2	50	50
Grooving in the outer race	6	0.2	50	50

Following the steps in Section 3, we firstly utilized the proposed HLZC method to extract the fault features. Then, the obtained features were fed into SVM for classification. The obtained results are shown in Figure 13. It can be seen from 0 that 16 samples were misclassified and the final accuracy was 94.67%. For comparison, the MLZC and LZC were also tested. To avoid randomness, we carried out 20 trials. Figure 14 and Table 2 illustrate the detailed recognition results using three methods. First, the proposed HLZC method achieved the highest average classification accuracy of 94.3% (ranging from 91.33% to 95.67%). This can be attributed to the high frequency components considered in the HLZC method, which can contribute more information in the high frequency to generate a more accurate estimation of complexity. Second, the MLZC method obtained the second-highest average classification accuracy of 91.72% (ranging from 89.33% to 93.67%). Third, the LZC method had the lowest classification accuracy of 63.47% (ranging from 61.67% to 66.33%) due to the ineffectiveness of single analysis. It is indicated that HLZC had the best performance in extracting fault features among the three methods.

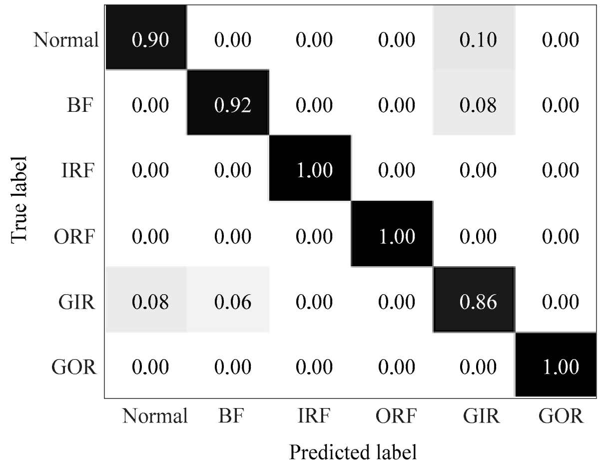

Figure 13. Confusion matrix using the proposed HLZC method for Experiment 1.

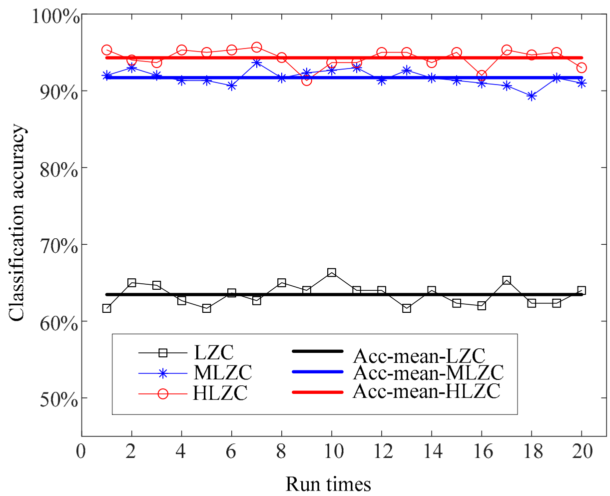

Figure 14. Diagnosis results of 20 trials using three methods in Experiment 1.

Table 2. Detailed classification accuracy of the experimental datasets in Experiment 1 and Experiment 2.

Experiments	**HLZC**			**MLZC**			**LZC**		
	Accuracy (%)			**Accuracy (%)**			**Accuracy (%)**		
	Max	**Min**	**Mean**	**Max**	**Min**	**Mean**	**Max**	**Min**	**Mean**
1	95.67	91.33	94.30	93.67	89.33	91.72	66.33	61.67	63.47
2	97.20	92	94.72	90	84.80	87.82	45.20	36	41.22

4.2. Experiment 2

Experiment 2 aimed to investigate the performance of HLZC in compound fault diagnosis of rotating machinery. Experiment 2 was composed of five compound fault types: health condition (Normal), broken tooth in the driving tooth with inner race fault (BI), missing tooth in the driving tooth with inner race fault (MI), health tooth in the driving tooth with inner race fault (NI), and pitting in the driving tooth with inner race fault (PI). There were 100 samples in each class and 500 samples in total. In addition, the data length was 2048 points. The waveforms under five working types are shown in Figure 15. The detailed information of five compound fault conditions is shown in Table 3.

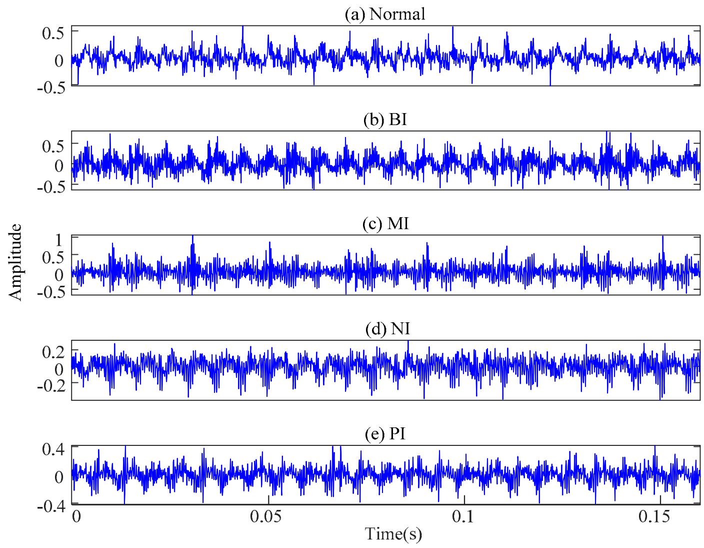

Figure 15. The time domain waveforms of rotating machinery in Experiment 2: (**a**) health condition (Normal), (**b**) broken tooth in the driving tooth with inner race fault (BI), (**c**) missing tooth in the driving tooth with inner race fault (MI), (**d**) health tooth in the driving tooth with inner race fault (NI), (**e**) pitting in the driving tooth with inner race fault (PI).

Table 3. Detailed information of five conditions in Experiment 2.

Fault Class	Class Label	Damage Diameter (mm)	Number of Training Samples	Number of Testing Samples
Normal	1	0	50	50
BI	2	0.01	50	50
MI	3	0.01	50	50
NI	4	0.01	50	50
PI	5	0.01	50	50

Like Experiment 1, the proposed HLZC-SVM method was also utilized for fault type identification of rotating machinery. Figure 16 shows the classification results. From Figure 16, we can see that there were a total of 10 samples misclassified with an accuracy of 96%. For comparison, the LZC and MLZC methods were also tested. The testing accuracies of the four methods are listed in Table 2 and Figure 17. As can be seen, the LZC-SVM was not effective, with an average classification accuracy of 41.22%. Second, combined with multi-scale analysis, the diagnosing performance of the MLZC-SVM method was enhanced with the average classification accuracy of 87.82%. Lastly, the proposed HLZC-SVM method had the highest average classification accuracy of 94.72%.

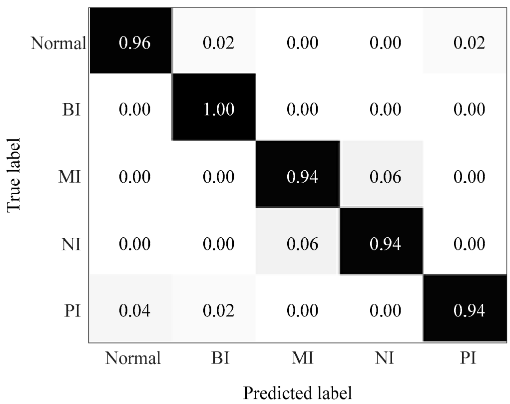

Figure 16. Confusion matrix using the proposed HLZC method for Experiment 2.

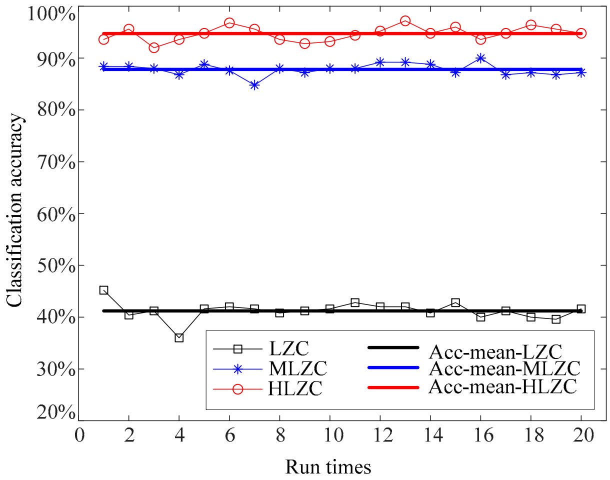

Figure 17. Diagnosis results of 20 trials using three methods in Experiment 2.

To better evaluate the classifier performance, we calculated the receiver operating characteristic (ROC) curves of HLZC-SVM, MLZC-SVM, and LZC-SVM methods using the experimental data. Here, we ran each method 20 times. The average ROC curve chart and AUC mean value of five health conditions of rotating machinery using three methods are shown in Figure 18. It can be observed from Figure 18a that our proposed HLZC-SVM method had the best performance with the highest AUC value for five health conditions (Normal with 1, BI with 1, MI with 0.99, NI with 0.99, and PI with 0.99). In contrast, the AUC values of MLZC-SVM and LZC-SVM for five health conditions showed a decreasing trend, as shown in Figure 18b,c, respectively. Among the three methods, the LZC-SVM method performed worst, in which the AUC values of five health conditions were only 0.5, 0.93, 0.53, 0.50, and 0.86. The comparison results further demonstrate that our proposed HLZC-SVM method had the best classification ability compared with the other two methods.

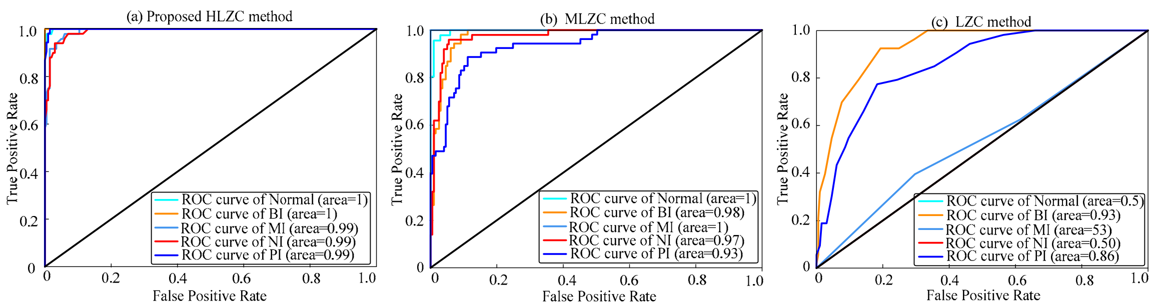

Figure 18. Performance comparison between three methods: (**a**) HLZC-support vector machine (SVM), (**b**) MLZC-SVM, and (**c**) LZC-SVM.

Moreover, random forest (RF) classifier was also applied for pattern identification for comparison. The ROC curve chart and AUC value were used to evaluate classification performance. Figure 19 shows average ROC curve chart and AUC mean value after running 20 times. As can be seen, the SVM classifier obtained a larger AUC value of 0.99 compared with RF classifier (AUC with 0.97), which meant the SVM had a better classification performance in recognizing various fault types of rotating machinery.

To gain a clear sense of the cluster ability of the extracted features using HLZC and MLZC methods, we used two-dimensional projection for visualization with PCA, as drawn in Figure 20. In 0a, it can be observed that the HLZC features of the five health conditions had a clear boundary and each cluster was individually separate. However, for the MLZC method, a few features were mixed, resulting in difficulty for classification. This phenomenon indicated that the fault features extracted using HLZC had more cluster ability than the MLZC method.

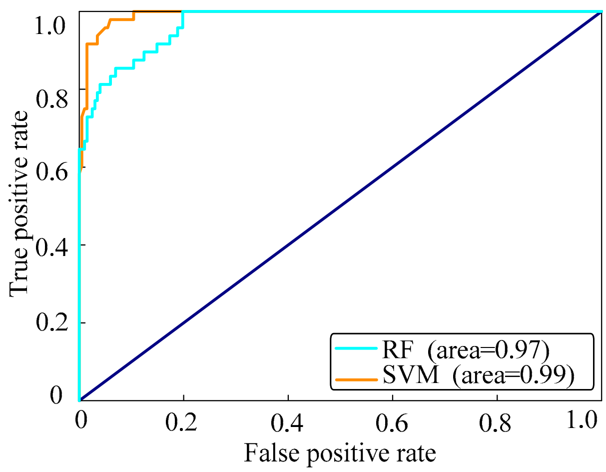

Figure 19. Performance comparison for different random forest (RF) and SVM.

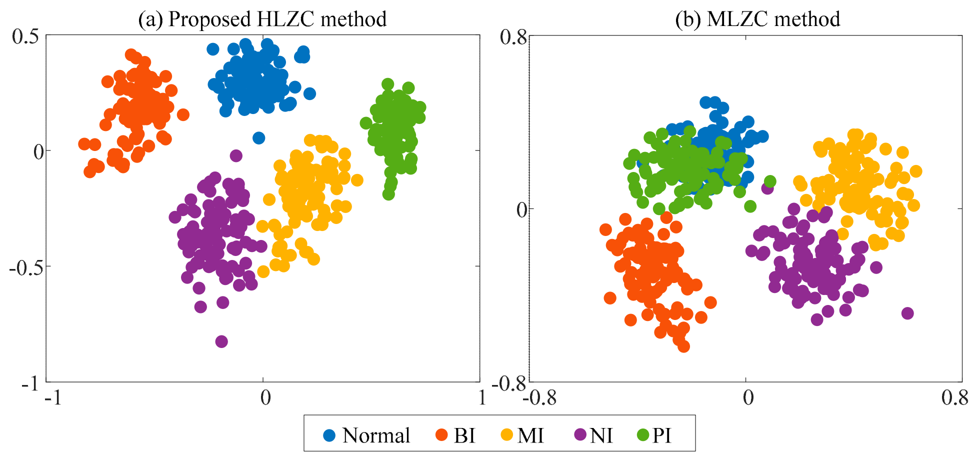

Figure 20. Projections of two-dimensional visualization of the obtained features in Experiment 2: (**a**) our proposed HLZC method, (**b**) traditional MLZC method.

We also tested the performance of our proposed HLZC method using different percentages of samples for training (the remaining samples will be considered as testing samples). Eight percentages were tested: 10% to 80%. To reduce randomness, 20 trials were conducted for each percentage. The averaging of training and testing accuracies were calculated and their corresponding standard deviations are illustrated in Figure 21. When the percentage increased to 50%, it achieved the highest classification accuracy at 94.72%. Therefore, we selected 50% of samples for training to demonstrate the advantage of our proposed HLZC method.

In order to discuss the influence of layer k, we applied the data of Experiment 2 for validation. Figure 22 shows the obtained classification accuracies using different layer k. As can be seen, when the layer $k < 4$, the classification accuracy will be significantly enhanced as the layer k rises. However, a larger layer k will greatly enhance the central processing unit (CPU) time. We observed that when the layer $k = 4$ increased to 5, the obtained classification accuracy was only improved by 0.08% from 94.72% (layer $k = 4$) to 94.80% (layer $k = 5$). However, the CPU time for layer $k = 5$ was 2116 s, which was almost double that of layer $k = 4$ at 1095 s.

Moreover, there was one extremely useful byproduct of RF—variable importance measures [33]—which was calculated to show the contribution of different components for the final classification accuracy, as shown in Figure 23. Note that a lager importance value indicated that the component had a greater influence on final predictions. It can be seen that X_{50} generated by layer $k = 5$ had a lower feature importance compared with that of component X_{40} generated by layer $k = 4$. This phenomenon further indicated that the additional features generated by HLZC with $k = 5$ had a small contribution on the final classification accuracy, which was well consistent with the classification results in Figure 22. Considering both the classification accuracy and CPU time, we selected the layer $k = 4$ for HLZC in this study.

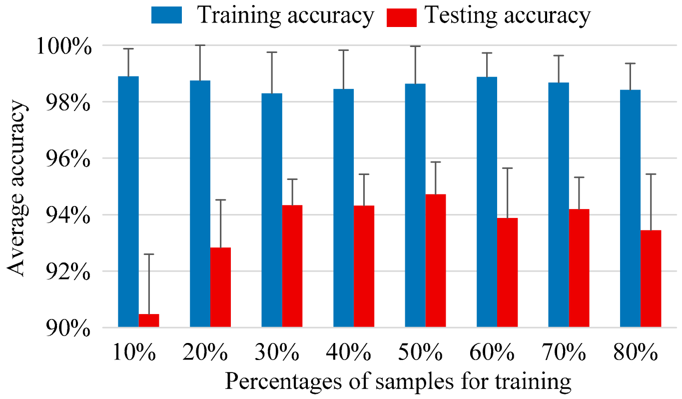

Figure 21. The classification results of the proposed method using training by different percentages of samples.

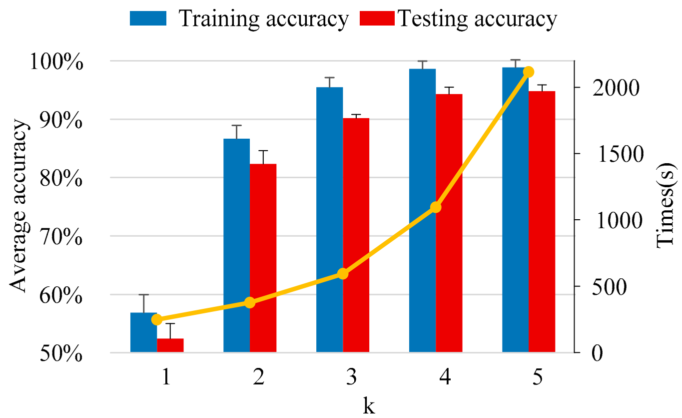

Figure 22. The mean classification accuracy and computation time using HLZC with different k.

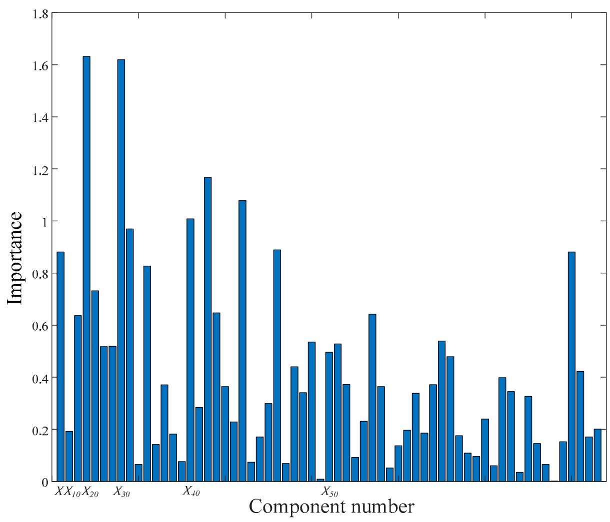

Figure 23. The importance of each component for the HLZC method.

For the MLZC method, we calculated the importance of each scale to show the contribution of different scales using data collected from Experiment 2. The obtained results are shown in Figure 24. It is worth mentioning that a lager importance value indicates that the component has a greater influence on final predictions. It can be seen that when the scale factor $\tau > 20$, the feature importance values of components showed a decreasing trend. This phenomenon indicated that the larger scale components ($\tau > 20$) had a small contribution on the final classification accuracy.

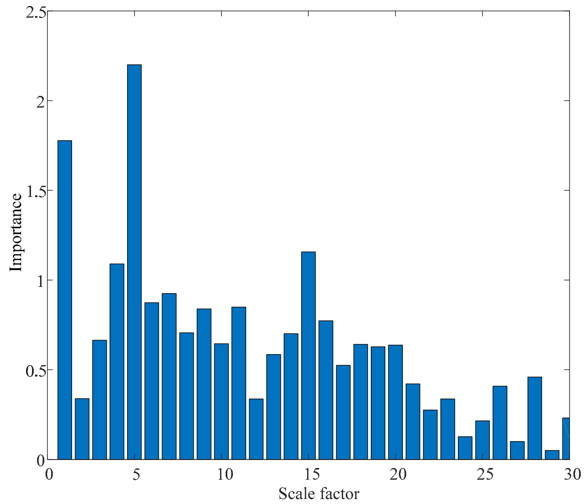

Figure 24. The importance of each scale factor for the MLZC method.

Additionally, the data of Experiment 2 were applied for validation to discuss the influence of scale factor τ. To reduce randomness, we conducted 20 trials conducted for each percentage. The testing accuracies were calculated and their corresponding CPU time is illustrated in Figure 25 and Table 4. As can be seen, when $\tau < 21$, the classification accuracy will be significantly enhanced as τ rises. When scale factor $\tau = 20$, it achieves the highest classification accuracy with 87.82%. Moreover, the larger scale means low calculation efficiency; thereby, we set scale factor $\tau = 1{:}20$ in this paper.

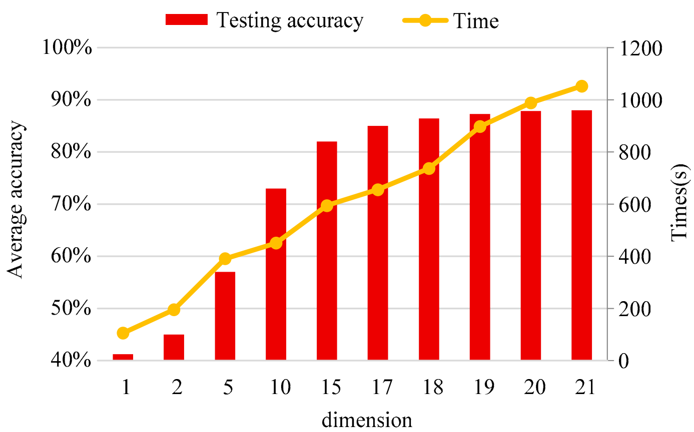

Figure 25. The mean classification accuracy and computation time using MLZC with different scale factor τ.

Table 4. Detailed classification accuracy of the experimental data using different scale factor τ.

Scale Factor τ	1	2	5	10	15	17	18	19	20	21
Max (%)	45.2	52	60	75	85	88	89	90	90	90
Min (%)	36	43	52	70	78	82	84	83	85	85
Mean (%)	41.22	45	57	73	82	85	86.4	87.2	87.82	87.2

5. Conclusions

A novel complexity analysis algorithm called HLZC was proposed for fault diagnosis of rotating machinery. The proposed HLZC can extract the fault information hidden in both low and high frequency components through the hierarchical decomposition. After the fault extraction, we utilized the SVM classifier to recognize different fault types of rotating machinery. To evaluate the performance of the proposed HLZC-SVM method, we used one simulated signal and two experimental signals with different fault types to verify the effectiveness of the HLZC-SVM method in FDRM. The comparison results demonstrated that the proposed HLZC-SVM method yielded the highest average classification accuracy of 94.3% and 94.72% for two cases, which was significantly higher than that of the LZ-SVM method (63.47% and 41.22%) and the MLZC-SVM method (91.72% and 87.82%). This further reinforces the fact that HLZC has certain advantages in fault feature extraction of rotating machinery. The main contributions of this paper include:

(1) LZC was extended to hierarchical decomposition analysis, namely, HLZC;
(2) HLZC considered the fault information hidden in both low-frequency and high-frequency components through conducting the averaging and differencing operations;
(3) A novel fault diagnosis scheme was proposed by combining HLZC and SVM;
(4) The proposed method was verified using both simulated and experimental signals.

There were some limitations for the proposed HLZC in fault diagnosis applications. First, although the proposed HLZC was demonstrated to be effective for the fault diagnosis of rotating machinery, it requires a large amount of labeled data for feature extraction and training the intelligent model for classification, which is difficult to meet sufficient labeled requirement in real industrial application scenarios. This limitation can be overcome by combing the feature knowledge transfer strategy with HLZC in future work. Second, the proposed HLZC lacks the denoising process to remove strong background noises so that it is difficult to extract the weak fault features from the strong noisy signal, especially at the early fault stage. This issue can hopefully be solved by applying the symbolic dynamic filtering to remove the noise-related fluctuations and reverse the fault-related information in future work.

Author Contributions: B.H. conceived the paper. B.H. and S.W. processed the data and wrote the paper. Q.Z. and X.Y. edited the manuscript. Y.L. helped to refined the whole paper and complete the final submission. All authors have read and agree to the published version of the manuscript.

Funding: This research was funded by the Key Project of National Natural Science Foundation of China (grant no. 51535009), the 111 Project (grant no. B13044), and the National Natural Science Foundation of China under grant 51805434, and in part by the Key Research Program, Shaanxi Province under grant 2019KW-017.

Conflicts of Interest: The authors declare no conflict of interest.All authors have read and agreed to the published version of the manuscript.

References

1. Liu, R.; Yang, B.; Zio, E.; Chen, X. Artificial intelligence for fault diagnosis of rotating machinery: A review. *Mech. Syst. Signal Process.* **2018**, *108*, 33–47. [CrossRef]
2. Li, Y.; Liu, F.; Wang, S.; Yin, J. Multi-scale Symbolic Lempel-Ziv: An Effective Feature Extraction Approach for Fault Diagnosis of Railway Vehicle Systems. *IEEE Trans. Ind. Inform.* **2020**, 1. [CrossRef]
3. Feng, Z.; Chen, X.; Liang, M. Iterative generalized synchrosqueezing transform for fault diagnosis of wind turbine planetary gearbox under nonstationary conditions. *Mech. Syst. Signal Process.* **2015**, *52*, 360–375. [CrossRef]
4. Abdeljaber, O.; Avci, O.; Kiranyaz, S.; Gabbouj, M.; Inman, D.J. Real-time vibration-based structural damage detection using one-dimensional convolutional neural networks. *J. Sound Vib.* **2017**, *388*, 154–170. [CrossRef]
5. Elasha, F.; Greaves, M.; Mba, D.; Fang, D. A comparative study of the effectiveness of vibration and acoustic emission in diagnosing a defective bearing in a planetry gearbox. *Appl. Acoust.* **2017**, *115*, 181–195. [CrossRef]

6. Sharma, R.B.; Parey, A. Modelling of acoustic emission generated due to pitting on spur gear. *Eng. Fail. Anal.* **2018**, *86*, 1–20. [CrossRef]
7. Zhao, M.; Lin, J. Health Assessment of Rotating Machinery Using a Rotary Encoder. *IEEE Trans. Ind. Electron.* **2018**, *65*, 2548–2556. [CrossRef]
8. Peng, Z.; Tse, P.W.; Chu, F. An improved Hilbert–Huang transform and its application in vibration signal analysis. *J. Sound Vib.* **2005**, *286*, 187–205. [CrossRef]
9. Li, G.; Tang, G.; Wang, H.; Wang, Y. Blind source separation of composite bearing vibration signals with low-rank and sparse decomposition. *Measurement* **2019**, *145*, 323–334. [CrossRef]
10. Qin, Y. A New Family of Model-Based Impulsive Wavelets and Their Sparse Representation for Rolling Bearing Fault Diagnosis. *IEEE Trans. Ind. Electron.* **2018**, *65*, 2716–2726. [CrossRef]
11. Li, J.; Yao, X.; Wang, H.; Zhang, J. Periodic impulses extraction based on improved adaptive VMD and sparse code shrinkage denoising and its application in rotating machinery fault diagnosis. *Mech. Syst. Signal Process.* **2019**, *126*, 568–589. [CrossRef]
12. Zheng, J.; Pan, H.; Cheng, J. Rolling bearing fault detection and diagnosis based on composite multiscale fuzzy entropy and ensemble support vector machines. *Mech. Syst. Signal Process.* **2017**, *85*, 746–759. [CrossRef]
13. Yan, R.; Gao, R. Complexity as a Measure for Machine Health Evaluation. *IEEE Trans. Instrum. Meas.* **2004**, *53*, 1327–1334. [CrossRef]
14. Yan, R.; Gao, R.X. Approximate Entropy as a diagnostic tool for machine health monitoring. *Mech. Syst. Signal Process.* **2007**, *21*, 824–839. [CrossRef]
15. Zheng, J.; Cheng, J.; Yang, Y.; Luo, S. A rolling bearing fault diagnosis method based on multi-scale fuzzy entropy and variable predictive model-based class discrimination. *Mech. Mach. Theory* **2014**, *78*, 187–200. [CrossRef]
16. Yan, R.; Liu, Y.; Gao, R.X. Permutation entropy: A nonlinear statistical measure for status characterization of rotary machines. *Mech. Syst. Signal Process.* **2012**, *29*, 474–484. [CrossRef]
17. Zheng, J.; Pan, H.; Yang, S.; Cheng, J. Generalized composite multiscale permutation entropy and Laplacian score based rolling bearing fault diagnosis. *Mech. Syst. Signal Process.* **2018**, *99*, 229–243. [CrossRef]
18. Li, Y.; Yang, Y.; Li, G.; Xu, M.; Huang, W. A fault diagnosis scheme for planetary gearboxes using modified multi-scale symbolic dynamic entropy and mRMR feature selection. *Mech. Syst. Signal Process.* **2017**, *91*, 295–312. [CrossRef]
19. Wu, S.-D.; Wu, C.-W.; Lin, S.-G.; Lee, K.-Y.; Peng, C.-K. Analysis of complex time series using refined composite multiscale entropy. *Phys. Lett. A* **2014**, *378*, 1369–1374. [CrossRef]
20. Hong, H.; Liang, M. Fault severity assessment for rolling element bearings using the Lempel–Ziv complexity and continuous wavelet transform. *J. Sound Vib.* **2009**, *320*, 452–468. [CrossRef]
21. Cui, L.; Gong, X.; Zhang, J.; Wang, H. Double-dictionary matching pursuit for fault extent evaluation of rolling bearing based on the Lempel-Ziv complexity. *J. Sound Vib.* **2016**, *385*, 372–388. [CrossRef]
22. Cui, L.; Li, B.; Ma, J.; Jin, Z. Quantitative trend fault diagnosis of a rolling bearing based on Sparsogram and Lempel-Ziv. *Measurement* **2018**, *128*, 410–418. [CrossRef]
23. Bai, Y.; Liang, Z.; Li, X. A permutation Lempel-Ziv complexity measure for EEG analysis. *Biomed. Signal Process. Control.* **2015**, *19*, 102–114. [CrossRef]
24. Yin, J.; Xu, M.; Zheng, H. Fault diagnosis of bearing based on Symbolic Aggregate approXimation and Lempel-Ziv. *Measurement* **2019**, *138*, 206–216. [CrossRef]
25. Li, Y.; Xu, M.; Wei, Y.; Huang, W. A new rolling bearing fault diagnosis method based on multiscale permutation entropy and improved support vector machine based binary tree. *Measurement* **2016**, *77*, 80–94. [CrossRef]
26. Costa, M.; Goldberger, A.L.; Peng, C.-K. Multiscale Entropy Analysis of Complex Physiologic Time Series. *Phys. Rev. Lett.* **2002**, *89*, 068102. [CrossRef]
27. Li, Y.; Wang, S.; Deng, Z. Intelligent fault identification of rotary machinery using refined composite multi-scale Lempel–Ziv complexity. *J. Manuf. Syst.* **2020**. [CrossRef]
28. Li, Y.; Xu, M.; Wang, R.; Huang, W. A fault diagnosis scheme for rolling bearing based on local mean decomposition and improved multiscale fuzzy entropy. *J. Sound Vib.* **2016**, *360*, 277–299. [CrossRef]
29. Jiang, Y.; Peng, C.-K.; Xu, Y. Hierarchical entropy analysis for biological signals. *J. Comput. Appl. Math.* **2011**, *236*, 728–742. [CrossRef]

30. Elton, R.J.; Vasuki, P.; Mohanalin, J. Voice Activity Detection Using Fuzzy Entropy and Support Vector Machine. *Entropy* **2016**, *18*, 298. [CrossRef]
31. Li, Y.; Wang, X.; Si, S.; Huang, S. Entropy Based Fault Classification Using the Case Western Reserve University Data: A Benchmark Study. *IEEE Trans. Reliab.* **2020**, *69*, 754–767. [CrossRef]
32. Martínez-Morales, J.D.; Palacios-Hernández, E.R.; Campos-Delgado, D.U. Multiple-fault diagnosis in induction motors through support vector machine classification at variable operating conditions. *Electr. Eng.* **2016**, *100*, 59–73. [CrossRef]
33. Archer, K.J.; Kimes, R.V. Empirical characterization of random forest variable importance measures. *Comput. Stat. Data Anal.* **2008**, *52*, 2249–2260. [CrossRef]